



# Role of the western hemisphere warm pool in climate variability over the western North Pacific

Jae-Heung Park<sup>1</sup> · Jong-Seong Kug<sup>2</sup> · Soon-Il An<sup>3</sup> · Tim Li<sup>1,4</sup>

Received: 24 April 2018 / Accepted: 27 January 2019 / Published online: 2 February 2019  
© Springer-Verlag GmbH Germany, part of Springer Nature 2019

## Abstract

The climate variability in the Western North Pacific (WNP), which is surrounded by densely populated countries, is closely tied to the lives of the people in the East Asia in terms of climate and socioeconomics. Along with global warming, remarkable interannual and interdecadal variations in sea surface temperature (SST) and sea surface height have been observed in the WNP. Here we demonstrated that boreal summer SST variability in the western hemisphere warm pool (WHWP, a.k.a. Atlantic Warm Pool) near the Intra-Americas Sea, which is known as the second largest warm pool on the planet, has considerably contributed to the climate variability in the WNP in subsequent winter. This is possible due to westward propagation of Rossby waves associated with a WHWP-SST warming (cooling) in mid-summer to early fall season, which induces northerly (southerly) wind anomalies over the North Pacific. In the presence of northeasterly mean trade winds, the anomalous meridional winds interact with SST and precipitation anomalies. Such air-sea coupling processes gradually move equatorward and westward along the climatological migration of the Pacific Intertropical Convergence Zone, and it has finally an effect on the climate variability over the WNP in winter. Further diagnosis verifies that WHWP-WNP connection exists not only on interannual time scale but also on decadal time scale. The analysis using state-of-the-art climate models reasonably supports this argument. A better understanding of the WHWP influence is expected to improve forecasts for the WNP climate and assist socioeconomic development in the East Asia.

**Keywords** Western North Pacific · Western Hemisphere Warm Pool (Atlantic Warm Pool) · Air-Sea Coupling

## 1 Introduction

The western North Pacific (WNP), which is adjacent to the East China Sea, the South China Sea, and the Philippine Sea, has been regarded as a climatologically important region (Wang et al. 2000). Oceanographically, the Kuroshio Current which is the strongest western boundary current is located (Liu and Gan 2012), so that enormous heat is conveyed from the Tropics to the mid-latitudes through the WNP throughout the year. Atmospherically, convection and associated atmospheric teleconnection in the WNP are linked to the sea level pressure (SLP) system near Japan (Pacific-Japan pattern, Nitta 1987) and East Asia climate variability (Wang et al. 2000; Son et al. 2014; Kim and Kug 2018). In addition, anomalous meridional wind over the WNP is closely associated with the intensity of the East Asian winter monsoon (Li and Wang 2005; Chen et al. 2000).

Previous studies have mentioned that the WNP is one of the sensitive regions to the global warming (Carton et al. 2005; Cheng et al. 2008; Deser et al. 2010; Williams

✉ Jong-Seong Kug  
jskug1@gmail.com

<sup>1</sup> International Pacific Research Center, Department of Atmospheric Sciences, School of Ocean and Earth Science and Technology, University of Hawaii at Manoa, Honolulu, HI, USA

<sup>2</sup> Division of Environmental Science and Engineering, Pohang University of Science and Technology (POSTECH), 77 Cheongam-Ro, Nam-Gu, Pohang 790-784, South Korea

<sup>3</sup> Department of Atmospheric Sciences, Yonsei University, 50 Yonsei-ro, Seodaemun-gu, Seoul 120-749, South Korea

<sup>4</sup> Key Laboratory of Meteorological Disaster, Ministry of Education (KLME), Joint International Research Laboratory of Climate and Environmental Change (ILCEC), Collaborative Innovation Center on Forecast and Evaluation of Meteorological Disasters (CIC-FEMD), Nanjing University of Information Science and Technology, Nanjing, China

2012; Wu et al. 2012). For instance, a considerable SST warming in the WNP has been observed with intensified Kuroshio Current in recent decades under increasing greenhouse gases (Williams 2012; Wu et al. 2012). Observational records based on satellites data show faster sea level rise and SST warming in the WNP than in other subtropical regions (Carton et al. 2005; Cheng et al. 2008; Deser et al. 2010). Such SST warming and sea level rising trends are approximately twice greater than their respective global mean trends (Fig. 1). In combination with more frequent and intense storm surges, these SST increase and sea level rise are expected to have a dramatic impact on marine flora and fauna in this area, particularly in low-lying coastal and intertidal regions where widespread floods and coastal erosion are prevalent (Leatherman et al. 2000).

Recently, importance of the interannual variability in the WNP has been more emphasized. It is reported that along with the global warming SST variability near the Philippines and Taiwan in winter could trigger El Niño in subsequent winter by efficiently generating a westerly wind anomaly in the western equatorial Pacific (For convenience, seasons in this study follow those of the Northern Hemisphere) (Wang et al. 2012, 2013). It is also argued that atmospheric teleconnection related to the atmosphere–ocean interaction in the WNP could induce North Pacific Oscillation (NPO)/North Pacific Gyre Oscillation (NPGO) in the North Pacific in boreal winter (Park and An 2014; Park et al. 2017). Additionally, Hartmann (2015) showed that interannual WNP-SST variability has been increasing, and its associated atmospheric teleconnection is significantly responsible for recent cold winters in the North America.

Above studies have addressed climatological importance of the WNP, implying that it is necessary to investigate a cause of interannual and decadal variability of WNP-SST. Although some efforts has been already put in order to understand the variability of the WNP (Liu and Gan 2012; Yeh and Kim 2010; Park et al. 2017), research on this is still insufficient, and less is known about what determines it.

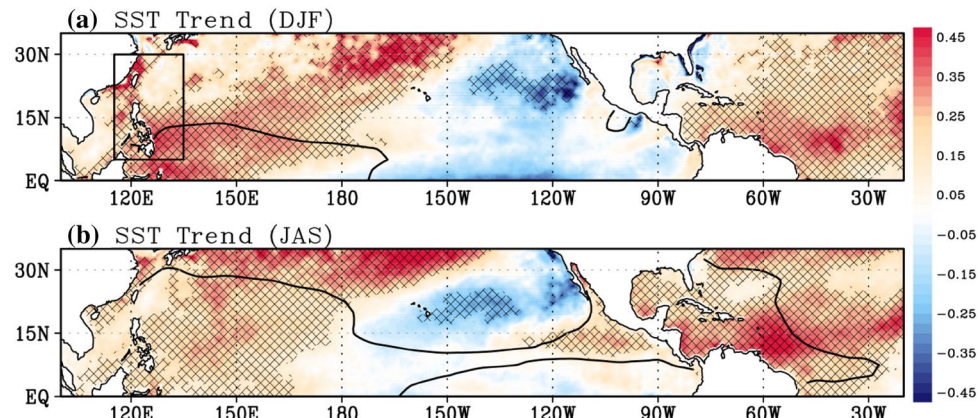
**Fig. 1** Trends of SST in **a** winter (DJF) and **b** mid-summer to early fall (JAS) during 1982–2014 ( $^{\circ}\text{C}/10 \text{ year}$ ) based on the OISST. In **a**, a black box indicates a WNP region for a definition of a WNP index. Solid black contours in **(a)** and **(b)** mark warm pool boundaries ( $> 28 ^{\circ}\text{C}$ ). Hatching indicates a 95% confidence level

In the meantime, a role of the Atlantic in Pacific climate modulation has been spotlighted (Ham et al. 2013a, b, 2017; McGregor et al. 2014; Yu et al. 2015; Li et al. 2016; Park et al. 2018a, b). From this perspective, we tried to investigate the Atlantic influence on the climate variability in the WNP, especially focusing on the western hemisphere warm pool (WHWP named by Wang and Enfield (2001), a.k.a. Atlantic Warm Pool) which is the second largest warm pool ( $> 28 ^{\circ}\text{C}$ ) on the globe as located near far eastern Pacific and Intra-Americas Sea (IAS). This is because the WHWP is located closer to the North Pacific than any other region in the Atlantic and its absolute SST is highest in the Atlantic. This implies that there is a good possibility for efficient teleconnection toward the Pacific. The WHWP reaches its areal and its variability maximums in mid-summer and early fall (Wang et al. 2006). In the season, expanding toward the North Tropical Atlantic (NTA), the WHWP has a large impact on the generation of hurricanes and precipitation over the northern South America and the Sahel over the eastern Africa (Wang and Enfield 2001; Wang et al. 2006).

The structure of this paper is organized as follows. Data-sets used in this study are described in the next section. In Sect. 3, we examine trends of SST and sea surface height (SSH) in the Pacific and Atlantic. Effect of the WHWP on climate over the WNP in observation and climate models are discussed in the Sect. 4 and 5, respectively. A summary and discussion are given in the last section.

## 2 Data and methods

Several reanalysis datasets were used to analyze the relationship between the WHWP and the WNP. For SST, we selected the Extended Reconstructed Sea Surface Temperature version 3 (ERSSTv3) from National Oceanic and Atmospheric Administration (NOAA) (Reynolds et al. 2007), which is based on a statistical interpolation of the International Comprehensive Ocean–Atmosphere Data Set



(ICOADS) release 2.4 data. The Optimum Interpolation Sea Surface Temperature version 2 (OISSTv2) from NOAA (Reynolds et al. 2002), characterized by very high resolution,  $0.25^\circ \times 0.25^\circ$ , was also used in Fig. 1 to complement the relatively low resolution ERSSTv3. The analysis period of OISSTv2 is 1982–2014. For SSH, we used the Reconstructed Sea Level Version 1 from National Aeronautics and Space Administration (NASA) ([https://podaac.jpl.nasa.gov/dataset/RECON\\_SEA\\_LEVEL\\_OST\\_L4\\_V1](https://podaac.jpl.nasa.gov/dataset/RECON_SEA_LEVEL_OST_L4_V1)), which is derived from not only tide gauges but also satellite altimetry with horizontal resolutions of  $0.5^\circ \times 0.5^\circ$  (Hamlington et al. 2014), of which period is 1979–2009. Altimetric records from multiple satellites are used since 1993, which provide accurate measurements of sea level with near-global coverage. It is noted that the period of TOPEX/Poseidon satellite is 1993–2006, of which data is known to be reliable (<https://sealevel.jpl.nasa.gov/missions/topex/>). To examine subsurface processes in ocean, Global Ocean Data Assimilation System (GODAS) from National Centers for Environmental Prediction (NCEP) which spans from 1980 to present is adapted (Behringer and Xue 2004). GODAS is known as a real-time ocean analysis and a reanalysis with high resolution (360-longitude, 418-latitude, 40-level). For analysis of atmosphere and precipitation, NCEP/NCAR Reanalysis 1 (NCEP-R1) (Kistler et al. 2001) and Global Precipitation Climatology Project version 2.1 (GPCPv2.1) (Huffman et al. 2009) were used, where their horizontal resolutions are  $2.5^\circ \times 2.5^\circ$ . In this study, the analysis period is basically from 1979 to 2015, but it could vary according to the data coverage.

We also analyzed state-of-the-art climate models participated in Coupled Model Intercomparison Project Phase (CMIP) 5. More than 30 models from the historical (1950–2000) and RCP4.5 (2010–2100) experiments (Ensemble 1) were used for the CMIP5 analysis; these models are listed in Table 1.

### 3 Trends of SST in the Pacific and Atlantic

SST trends in winter (December, January, February; hereafter DJF) and mid-summer to early fall (July to September; JAS) are first examined (Fig. 1a–b). In winter, significant SST warming trends at 95% confidence level are widely observed over the western Pacific and the central North Pacific (Fig. 1a). Note that the SST warming trends in the WNP are higher than those in other tropical to subtropical regions in the Pacific and the Atlantic. The maximum SST trend in the WNP is about  $0.35\text{ }^\circ\text{C}/10\text{ year}$ , indicating that WNP-SST has increased more than  $1\text{ }^\circ\text{C}$  over the last 30 years, which is consistent with a previous study (Lima and Wethey 2012). Interestingly, there seem two branches of significant SST warming trends starting from the Philippines:

one stretches toward the central North Pacific, and the other stretches toward the East China Sea along the path of the Kuroshio Current. For the latter, it could imply the important role of oceanic currents in the WNP-SST. Meanwhile, significant cooling trends occur off the coast of Baja California, contrasted with the warming trends in the central North Pacific. These cooling trends are connected to the equatorial eastern Pacific where La Niña-like SST trends are shown (An et al. 2012; Chung and Li 2013; Merrifield 2011; Whitmarsh et al. 2015). In the Atlantic, significant warming trends are also seen over wide regions, except the Gulf of Mexico and the Gulf Stream.

In summer, the area of significant warming trends in the Atlantic expands toward the western North America (Fig. 1b). The highest warming trends in the Atlantic are observed along the coastline of the northern South America to the Central America. Significant warming trends are also seen over the western coast of the Central America; therefore, significant warming trends are located at both sides of the Central America. A solid black line in Fig. 1b indicates a warm pool boundary in which the climatological mean SST is higher than  $28\text{ }^\circ\text{C}$ . The Indo-Pacific warm pool is linked to the Atlantic through a latitudinally narrow band over the eastern Pacific that coincides with the Intertropical Convergence Zone (ITCZ). Around the Atlantic, the WHWP is located over the off-equatorial regions in the far eastern Pacific and IAS. Since significant SST trends are observed in the WHWP during JAS, it is deduced that absolute SST in WHWP has considerably increased during the recent decades.

## 4 Effect of WHWP on climate over the WNP

### 4.1 Interannual perspective

To understand what contributes to interannual variability of WNP-SST in winter, we defined a WNP index as an areal-average of SST in  $115^\circ\text{--}135^\circ\text{E}$ ,  $5^\circ\text{--}30^\circ\text{N}$  (a black box in Fig. 1a) in winter (D0JF1), hereafter the number denotes order of year). Based on the WNP index, we conducted a lagged correlation analysis with SST in the previous JAS(0). As shown in Fig. 2a, significant correlation coefficients locate around the WNP, the WHWP, and the Hawaiian Islands. It is noteworthy that the highest correlation coefficients appear in the WHWP, not around the WNP. It means that winter WNP-SST is closely correlated to the preceding summer WHWP-SST, implying a delayed impact of WHWP-SST on WNP-SST. On the basis of the result, we defined an another index (a WHWP index) to represent summer WHWP-SST variability by areal-averaging of summer SST (JAS) in the WHWP ( $60^\circ\text{--}105^\circ\text{W}$ ,  $10^\circ\text{--}35^\circ\text{N}$ , as shown by a black box in Fig. 2a). It should be mentioned that there

**Table 1** Models used in this study from the historical and RCP4.5 experiments in CMIP5

| Model name     | Modeling center (or group)  | Hist. | RCP4.5 |
|----------------|---|-------|--------|
| ACCESS1-0      | CSIRO (Commonwealth Scientific and Industrial Research Organisation, Australia), and BOM (Bureau of Meteorology, Australia)   | O     | O      |
| ACCESS1-3      |   |       | O      |
| BCC-CSM1-1     | Beijing Climate Center, China Meteorological Administration   | O     |        |
| BCC-CSM1-1-m   |   | O     |        |
| CanESM2        | Canadian Centre for Climate Modelling and Analysis  | O     | O      |
| CCSM4          | National Center for Atmospheric Research  | O     | O      |
| CESM1-BGC      | National Science Foundation, Department of Energy, National Center for Atmospheric Research   | O     |        |
| CESM1-CAM5     |   | O     | O      |
| CNRM-CM5       | Centre National de Recherches Meteorologiques   | O     | O      |
| CMCC-CESM      | Centro Euro-Mediterraneo per I Cambiamenti Climatici  | O     |        |
| CMCC-CM        |   | O     | O      |
| CMCC-CMS       |   | O     | O      |
| CSIRO-Mk3-6-0  | Commonwealth Scientific and Industrial Research Organisation in collaboration with the Queensland Climate Change Centre of Excellence                                     | O     | O      |
| EC-EARTH       | EC-EARTH consortium   | O     | O      |
| FGOALS-g2      | LASG, Institute of Atmospheric Physics, Chinese Academy of Sciences; and CESS, Tsinghua University  | O     |        |
| FGOALS-s2      | LASG, Institute of Atmospheric Physics, Chinese Academy of Sciences   | O     |        |
| FIO-ESM        | The First Institute of Oceanography, SOA, China   | O     |        |
| GFDL-CM3       | NOAA Geophysical Fluid Dynamics Laboratory  | O     | O      |
| GFDL-ESM2G     |   | O     | O      |
| GFDL-ESM2M     |   | O     | O      |
| GISS-E2-H      | NASA Goddard Institute for Space Studies  | O     | O      |
| GISS-E2-H-CC   |   |       | O      |
| GISS-E2-R      |   | O     | O      |
| GISS-E2-R-CC   |   |       | O      |
| HadCM3         | Met Office Hadley Centre (additional HadGEM2-ES realizations contributed by Instituto Nacional de Pesquisas Espaciais)  | O     |        |
| HadGEM2-AO     | Met Office Hadley Centre  | O     | O      |
| HadGEM2-CC     |   | O     | O      |
| HadGEM2-ES     |   | O     | O      |
| INMCM4         | Institute of Numerical Mathematics, Russian Academy of Sciences   | O     | O      |
| IPSL-CM5A-LR   | Institute Pierre Simon Laplace  | O     | O      |
| IPSL-CM5A-MR   |   |       | O      |
| MIROC5         | Atmosphere and Ocean Research Institute (The University of Tokyo), National Institute for Environmental Studies, and Japan Agency for Marine–Earth Science and Technology | O     | O      |
| MIROC-ESM      | Japan Agency for Marine–Earth Science and Technology, Atmosphere and Ocean Research Institute (The University of Tokyo), and National Institute for Environmental Studies | O     | O      |
| MIROC-ESM-CHEM |   |       | O      |
| MPI-ESM-LR     | Max Planck Institute for Meteorology  | O     | O      |
| MPI-ESM-MR     |   |       | O      |
| MRI-CGCM3      | Meteorological Research Institute   | O     | O      |
| MRI-ESM1       |   | O     |        |
| NorESM1-M      | Norwegian Climate Centre  | O     | O      |
| NorESM1-ME     |   | O     | O      |

are no significant differences in the results of this study even though JAS is changed into JJA or ASO as long as WHWP-SST is climatologically high.

The lagged correlation coefficient between WHWP-SST (JAS(0)) and WNP-SST (D(0)JF(1)) indices is significantly

high, 0.71 (Fig. 2b), which indicates that nearly half of the total variability of the winter WNP-SST can be linearly explained by the variability of WHWP-SST in previous summer. It is necessary to consider that such simple interpretation based on the linear correlation analysis could be

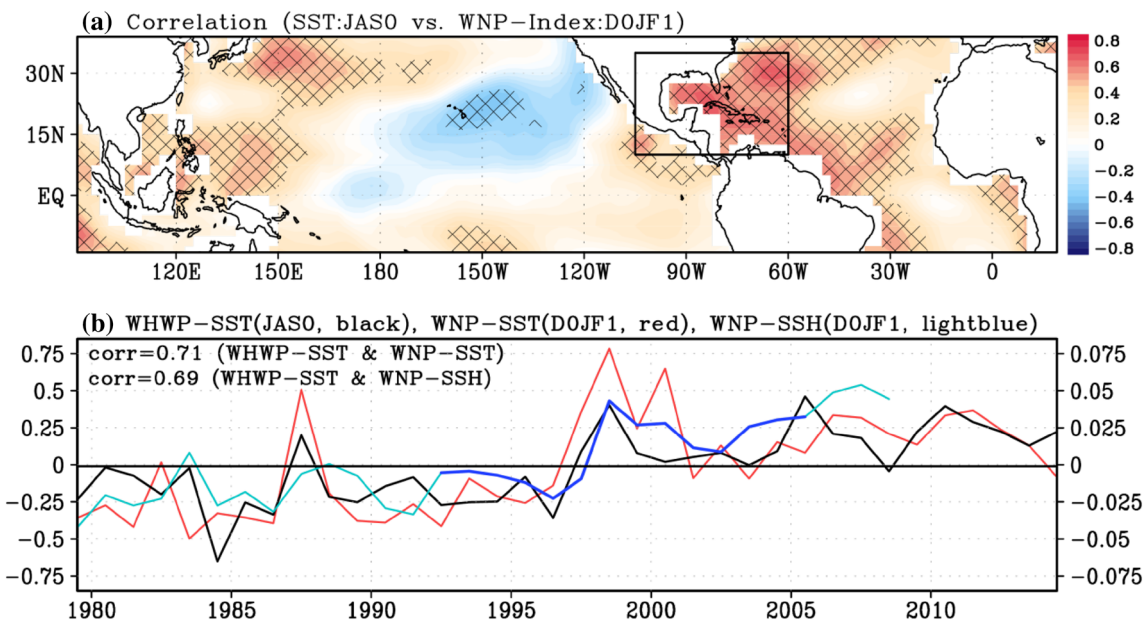


**Fig. 2** **a** A lagged correlation map of previous summer SST (JAS0) with the WNP-SST index (DOJF1). Hatching indicates a 95% confidence level, and color bar is shown at the right side. Here, a black box region is used to define the WHWP-SST index. **b** WHWP-SST, WNP-SST (left axis, °C), and WNP-SSH indices (right axis, m) are

indicated by the solid red, black, and lightblue lines, respectively. For the WNP-SSH index, the period of TOPEX/Poseidon satellite (1993–2006) is superposed by thick-blue line. The correlation coefficient between the WNP-SST (SSH) and WHWP-SST indices is 0.71 (0.69)

affected by the monotonic trends of both regions in winter and summer, respectively (Fig. 1). However, even when their trends are linearly removed or a 11-year high pass filter is applied to remove decadal signals, the correlation coefficients are 0.51 and 0.52, respectively, which is still significant at 95% confidence level. In a linear sense, these results indicate that variability of WHWP-SST is able to explain roughly 25% of total variability of WNP-SST.

At this moment, we tried to understand a quantitative role of WHWP-SST in WNP-SST trend by a linear regression method. Estimated trend of WNP-SST by WHWP-SST can be roughly obtained from below Eq. (1).

$$\text{Estimated Trend(WNP - SST)} = \text{Regression(WNP - SST, WHWP - SST)} \times \text{Trend(WHWP - SST)} \quad (1)$$

Since the observed and estimated trends of WNP-SST are  $0.019^{\circ}\text{C}/\text{yr}$  and  $0.015^{\circ}\text{C}/\text{yr}$ , it can be thought that 79% of observed trend of WNP-SST is explained by WHWP-SST in a linear sense.

It is needed to understand how summer WHWP-SST is able to influence subsequent winter WNP-SST with an approximately two-season lag. For this, a lead-lag correlation analysis with the WHWP index is conducted (Fig. 3). Before analysis, trends of all data are removed first in order to focus on the interannual variability. In ASO(0) (Fig. 3a), there are negative SLP anomalies in the

WHWP where the SST is anomalously high. Consistent with the high SST and negative SLP anomalies, positive precipitation anomalies occur in the WHWP (Fig. 3b). At this moment, Rossby waves are generated by atmospheric heating forcing associated with the positive precipitation anomaly, leading to low-level cyclonic anomalies in the eastern North Pacific to the western WHWP. As a result, at the western edge of the cyclonic circulation, northerly wind anomalies form over the subtropical North Pacific ( $150^{\circ}\text{W}$ – $180^{\circ}$ ,  $15^{\circ}$ – $30^{\circ}\text{N}$ ).

In order to examine whether the anomalous northerly wind is caused by the Rossby wave response to the atmos-

pheric heating over the WHWP, we conducted a linear baroclinic model (LBM) experiment (Watanabe and Kimoto 1999). For this experiment, an atmospheric heating is prescribed over the WHWP by referring the result in Fig. 3b (Fig. 4a), and atmospheric climatology in JAS is prescribed as a background. Steady responses to the heating forcing are shown in Fig. 4b, in which low-level northerly flows are located over the North Pacific. Therefore, it is concluded that the anomalous northerly wind over the North Pacific is a by-product of the Rossby wave response to the SST warming in the WHWP.

**Fig. 3** Interannual lagged correlation maps of primary variables against the WHWP index in a ASO(0) to h ND(0) J(1). **a** SST (shading, above 95% confidence level is shaded), SLP (contours, intervals of 0.2, above 95% confidence level is hatched), **b** precipitation (above 90, 95, and 99% confidence level is dotted, bigger dots indicate a higher confidence level), wind (vectors, shown above 95% confidence level), and climatological precipitation (shading) are shown. Panels in following rows are same as panels **a** and **b** but for the SON (**c**, **d**), OND (**e**, **f**), and NDJ (**g**, **h**), respectively. Note that trends of all data are removed first before calculation

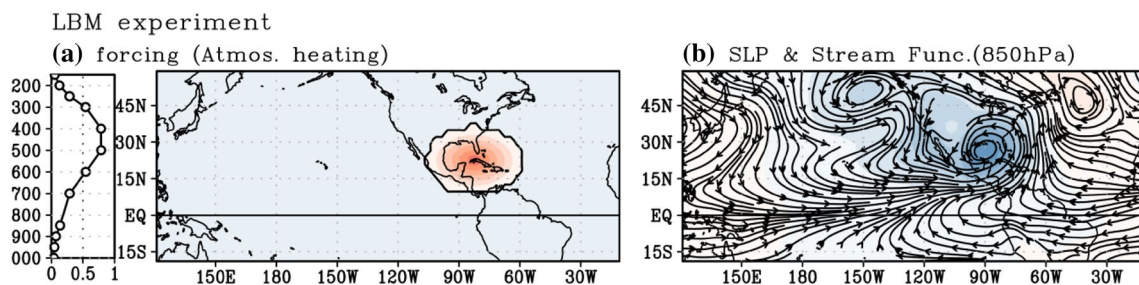
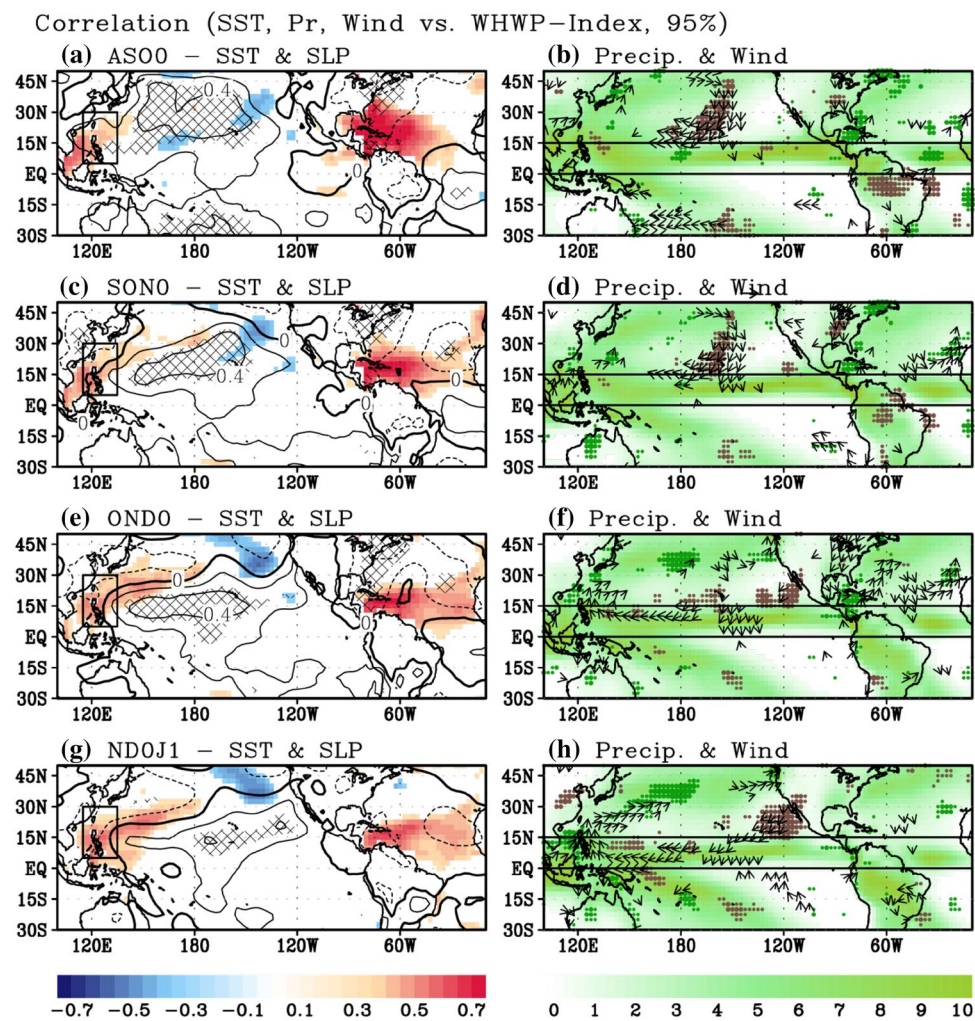


**Fig. 4** A linear baroclinic model experiment. **a** Atmospheric heating forcing and **b** its steady responses of SLP and stream function at 850 hPa. Atmospheric climatology of JAS is prescribed in the experiment as a basic state

Under the northeasterly mean trade winds, such a northerly wind anomaly contributes to sea surface cooling through increased surface evaporation by stronger wind speed (wind-evaporation-SST (WES) feedback) (Fig. 3a, b). At the same time, the northeasterly wind anomalies also bring dry and cold air (i.e., anomalous negative moist static energy advection), thus negative precipitation anomalies occur over the subtropical North Pacific. Since these negative precipitation

anomalies lead to anticyclonic anomalies over its western regions due to the Gill-type response, the anomalous northeasterly winds are relayed westward and equatorward in the subtropical Pacific (Fig. 3d, f, h). As the anomalous northeasterly wind expands westward, so does the negative precipitation anomaly. Therefore, the WHWP signals can be propagated to the western Pacific throughout late summer to winter. We note that such processes look similar to the

Pacific meridional mode (PMM) mechanism or the NTA-El Niño mechanism (Ham et al. 2013a). This is because north-easterly mean trade winds over the subtropical North Pacific are dominant all year around, so that such air-sea coupling processes can be active all the time.

Along the ITCZ where the convective activity is climatologically vigorous, air-sea coupling processes can be more active. During fall to winter when ITCZ migrates toward the equator, negative precipitation anomalies are co-located over ITCZ in the western Pacific (Fig. 3f, h). As the Gill-response to these negative precipitation anomalies, anticyclone circulation develops over the eastern Philippine Sea. Consequently, southerly wind anomalies are located over the western edge of the anticyclonic flow in the WNP in winter. Interacting with the northerly mean winds over the WNP in winter, the southerly wind anomaly reduces total wind speed over there, which leads to reduction in oceanic mixing and surface evaporation. It contributes to a SST warming around the Philippines as shown in Fig. 3e, g.

For better understanding of the WNP-SST warming, mixed-layer heat budget is conducted, where mixed-layer depth is assumed as 50 m (de Boyer Montégut et al. 2004). Figure 5 shows mixed-layer heat budget in the WNP ( $115^{\circ}$ – $135^{\circ}$ E,  $5^{\circ}$ – $30^{\circ}$ N) from August to subsequent January. Herein, it is known that temperature tendency is largely dominated by surface net heat flux (where, latent heat flux plays a dominant role). Horizontal and vertical temperature advects have relatively small contributions to the temperature tendency. But, horizontal temperature advection plays an important role in the SST warming along the Kuroshio Current path in November and December, contributed by both the enhanced Kuroshio Current and the intensified meridional temperature gradient ( $-\frac{dt}{dy}$ ) (not shown).

Anomalous negative wind-stress curl occurred near  $130^{\circ}$ – $160^{\circ}$ E in fall induces mass convergence by Ekman

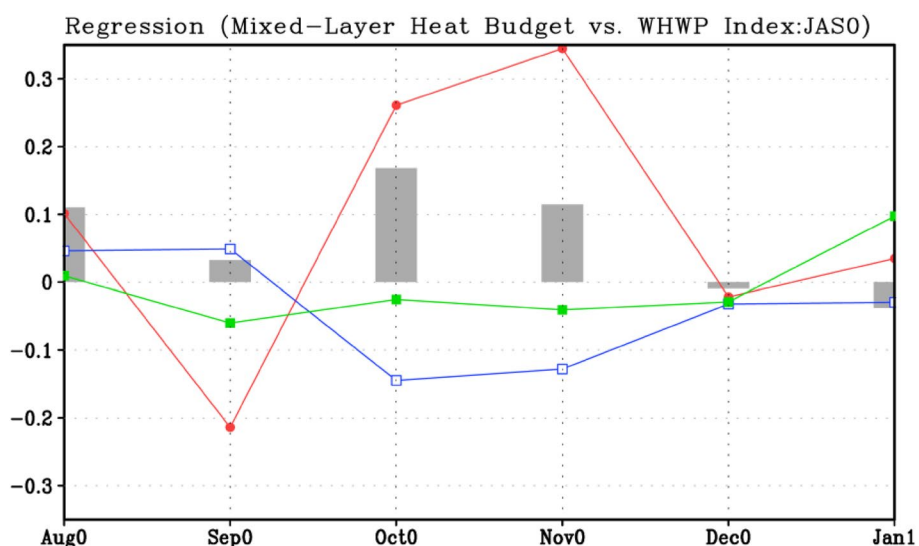
transport (Qiu 2003; Lysne and Deser 2001) (Fig. 6a). This windstress curl generates downwelling, leading to deepened thermocline depth. Such deepened thermocline depth is associated with higher SSH and subsurface temperature warming (Fig. 6b). Based on the result in Fig. 6, we define a WNP-SSH index using the areal average of the SSH in the WNP ( $120^{\circ}$ – $150^{\circ}$ E,  $15^{\circ}$ – $30^{\circ}$ N) in winter (Fig. 2b). The correlation coefficient between the WNP-SSH and WHWP-SST indices is 0.69 (Fig. 2b), which is significant at a 95% confidence level; when their trends are linearly removed or a 11-year high pass filter is applied to remove decadal signals, the correlation coefficient is 0.49 and 0.48, still significant at 95% confidence level. In a linear sense, these results indicate that WHWP-SST is able to explain roughly 25% of total variability of WNP-SSH. We also note that, during the TOPEX/Poseidon satellite period (1993–2005) which is considered to be reliable in its quality, the correlation coefficient increases further to 0.78 (0.70 for the detrended data). In short, the atmosphere–ocean coupled system over the North Pacific initiated by the WHWP-SST warming in summer contributes to the noticeable SST warming and SSH rise over the WNP in the following winter.

## 4.2 Decadal perspective

So far, interannual WHWP-WNP relationship is investigated, focusing on the WHWP in summer and the WNP in subsequent winter. Meanwhile, it is necessary to remind that there are strong decadal trends of SST in the WHWP and the WNP during summer and winter, respectively (Fig. 1). Motivated by above results, in this section we will examine a possible relationship between the WHWP and the WNP on a decadal time scale.

First, we examine whether above interannual dynamical mechanism operates similarly on a decadal time scale. For

**Fig. 5** Regression coefficients against the WHWP index from August to subsequent January regarding mixed-layer heat budget in the WNP ( $115^{\circ}$ – $135^{\circ}$ E,  $5^{\circ}$ – $30^{\circ}$ N). Gray bar indicates temperature tendency ( $^{\circ}$ C/month), and red, blue, and green solid lines indicate the warming/cooling by surface net heat fluxes ( $SW + LW + LH + SH$ ,  $^{\circ}$ C/month), horizontal temperature advection ( $-\nabla^{\text{w}} \cdot VT - (V^{\text{w}} \cdot \nabla)T$ ), and vertical temperature advection ( $-\nabla^{\text{h}} \cdot VT - (W^{\text{h}} \cdot \nabla)T$ ) ( $^{\circ}$ C/month). Here, mixed-layer depth is assumed as 50 m (de Boyer Montégut et al. 2004)



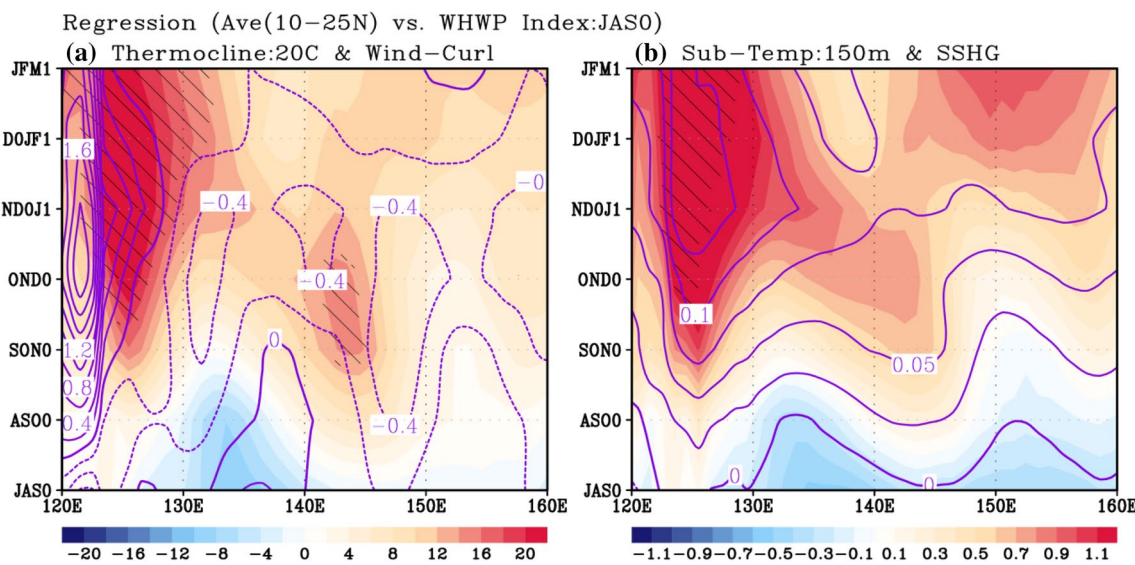


**Fig. 6** Regression coefficients of **a** thermocline depth anomaly (shading, m), wind stress curl anomaly (contour,  $\times 10^6 \text{ N/M}^3$ ) and **b** subsurface temperature anomaly ( $^{\circ}\text{C}$ ) at 150 m and anomalous SSH

(above geoid, m) along the  $10^{\circ}$ – $25^{\circ}\text{N}$  against the WHWP index. Hatching indicates confidence level at 90% of **a** thermocline and **b** subsurface temperature by two-tailed t-test

this, differences of several primary variables between the first (1979–1993) and the last fifteen (2001–2015) years are examined (Fig. 7), which reflects decadal trends during this period. In late summer (Fig. 7a, b), positive precipitation anomalies over the WHWP occur, and at the same time northerly wind, positive SLP, and negative precipitation anomalies locate over the eastern North Pacific. The northerly wind anomalies are linked to anticyclonic flows over the eastern Philippine Sea with anomalous negative precipitation (Fig. 7d, f, h). In terms of SLP, anomalous ridge is also found near the Philippine Sea (Fig. 7c, e, g). Along the western boundary of the ridge, there are anomalous southerly winds which contribute to SST warming (Fig. 7e, g). All of these features look similar to the developments of interannual WHWP influence on the WNP as indicated in Fig. 3. Therefore, it is concluded that such WHWP-WNP connection still holds on the decadal time scale as well as on the interannual time scale.

Furthermore, we also examined decadal relationship between WHWP and WNP by comparing their indices where 11-year-moving average is applied with longer period (ERSSTv3, ranging from 1854 to 2015) (Fig. 8). Herein, a significant relationship between WHWP and WNP on the decadal time scale is shown although there is discrepancy around 1960s.

## 5 WHWP-WNP relationship in CMIP5

Even though observational analysis showed a robust relationship between the WHWP and the WNP, more verification of the relationship using model data should be needed.

To support the observational results, we analyze datasets of state-of-the-art climate models that participated in the Coupled Model Intercomparison Project phase 5 (CMIP5). Here, total 33 model datasets from the historical experiment in CMIP5 were used, in which analyzed period is 1950–2000 (Table 1). Here SST is focused on rather than SSH.

First, the WHWP-WNP relationship is examined on an interannual scale (Fig. 9). For the multi-model ensemble, the correlation coefficient between the WHWP and WNP indices was 0.41, which is significant at 95% confidence level by a bootstrap method, even though it is smaller than the observational value. After removing trends from both indices, the correlation coefficient is slightly reduced to 0.35; however, it is still significant. This result shows that the current climate models tend to simulate the observed WHWP-WNP relationship. It is remarkable that all climate models show positive WHWP-WNP relationship, indicating that the results of CMIP5 models reasonably support the observational result. In particular, 28 models out of the 33 models show a significant correlation at 95% confidence level. This relationship is slightly weakened after trend is removed; however, 26 models still show a significant relationship.

In addition, it is examined how WHWP influences are conveyed into the North Pacific in CMIP5 models. We selected 10 models showing a good WHWP-WNP relationship based on the result of Fig. 9, where each model has a correlation coefficient greater than 0.5. In fall (Fig. 10), there are positive precipitation and negative SLP anomalies with a SST warming in the WHWP. In response to the WHWP signals, Rossby waves propagate toward the North Pacific, which induces northerly wind anomaly over the North

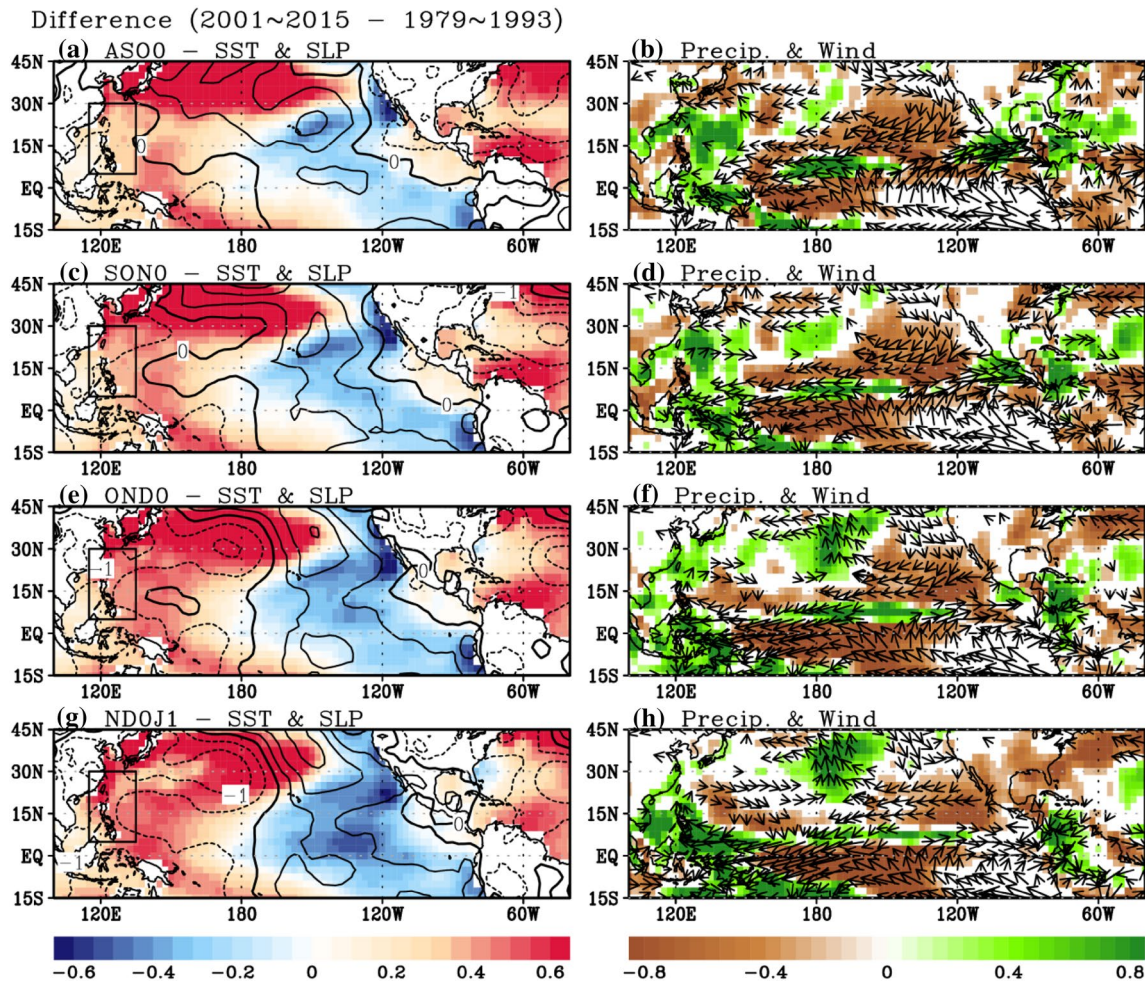


**Fig. 7** Differences of primary variables between first (1979–1993) and last fifteen (2001–2015) years, respectively. Top to bottom panels show the results in ASO(0), SON(0), OND(0) and ND(0)J(1), respec-

tively. Left panels illustrate SST (shading,  $^{\circ}\text{C}$ ) and SLP (contour, interval is 0.5 hPa). Right panels indicate precipitation (shading, mm/day) and wind (vector)

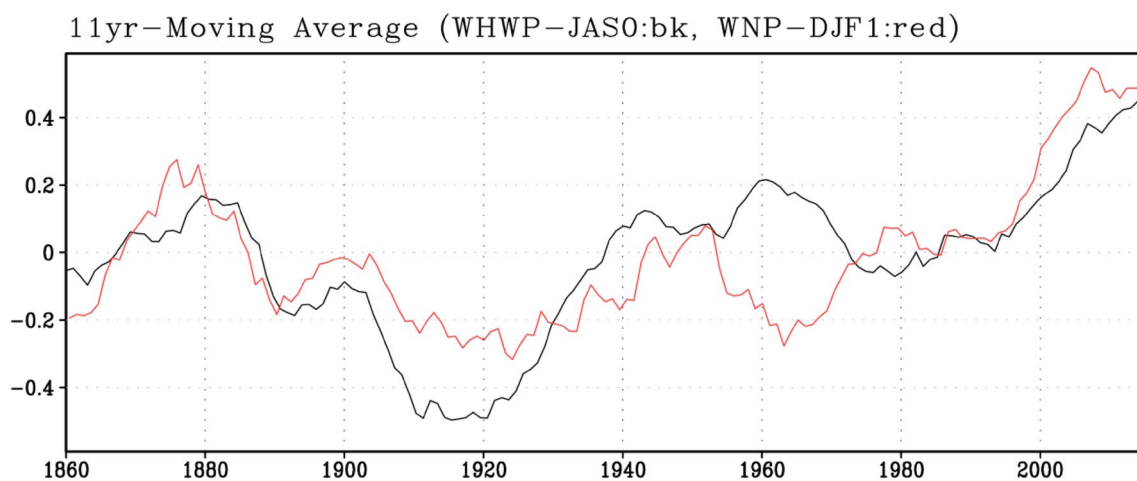


**Fig. 8** 11-year moving averages of summer WHWP-SST (JAS, black) and winter WNP-SST (DJF, red) during 1854–2015 ( $^{\circ}\text{C}$ , left axis)

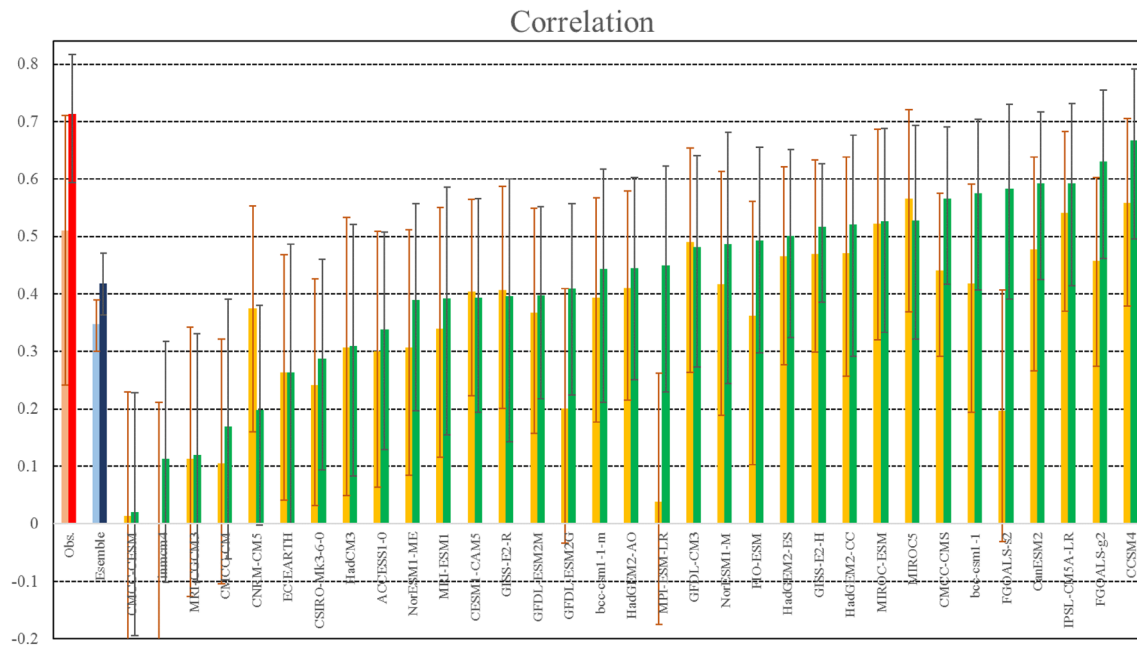


**Fig. 9** Correlation coefficients between the WHWP and WNP indices of CGCM models (historical run) in CMIP5 (green and yellow bars for trend and detrended cases). The error bars indicate a 95% confidence level calculated by a bootstrap method. The two leftmost bars

indicate observation (red and orange bars for the trend and detrended data) and model ensemble results (blue and sky blue bars for trend and detrended data)

Pacific. Related to the northerly wind, anomalous negative precipitation is widely located over the North Pacific. At the moment, a positive SLP anomaly is located over the

western to central North Pacific where is a western region of the northerly wind anomaly. Around the positive SLP anomaly, the anticyclonic circulation forms, corresponding

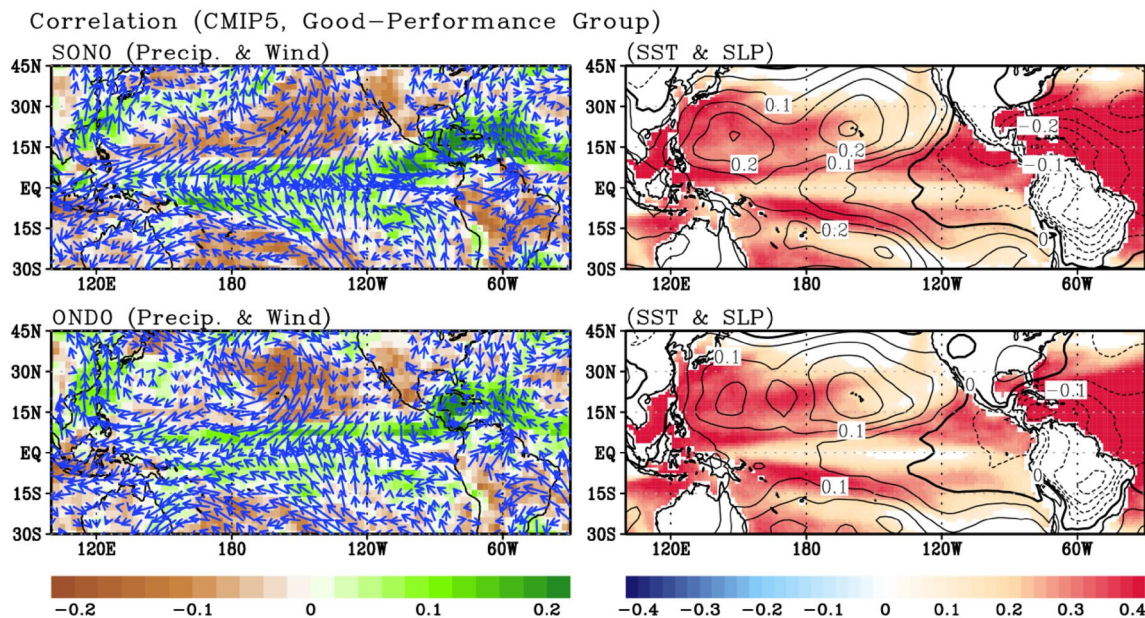


**Fig. 10** Ensemble of correlation coefficients from selected 10 models in CMIP5 against the WHWP index. Left panels shows precipitation (shading, mm/day) and low-level wind (vector), and right panels indicate SST (shading,  $^{\circ}$ C) and SLP (contour) for SON (top) and OND (bottom), respectively

cates SST (shading,  $^{\circ}$ C) and SLP (contour) for SON (top) and OND (bottom), respectively

to the southerly wind anomalies near the Philippines in fall to early winter. Then, WNP-SST can be warmed by reduced latent heat fluxes, as explained earlier section. Hence, overall features in CMIP5 models look similar to the result of the observation (Fig. 3) even though there are some differences.

Above result allows us to further investigate how long-term trends of WHWP-SST contribute to WNP-SST. To examine the relationship, long-term SST changes in the WHWP and the WNP is examined (Fig. 11a), which is defined as the difference (last minus first) between the first (1951–1965) and last 15-year (1986–2000). Here in order to remove a model dependency of global-mean sensitivity to the greenhouse warming, global mean SST ( $0^{\circ}$ – $360^{\circ}$ E,  $60^{\circ}$ S– $60^{\circ}$ N) in each model was removed. Models with a strong WHWP-SST warming in summer tend to simulate a strong WNP-SST warming in winter. The correlation coefficient in the inter-model space is 0.50, which is significant at a 95% confidence level. We applied the same analysis to the 32-model data from the RCP4.5 experiment (Table 1), and examined the SST differences in the WHWP and the WNP between the first (2011–2040) and last (2071–2100) 30-yr periods (Fig. 11b), where the global mean SST has been excluded as well. In the figure, significant relationship between WHWP-SST and WNP-SST is confirmed again. The correlation coefficients in the inter-model space are 0.61, implying the possibility that WHWP-SST warming trends in the future could enhance WNP-SST warming.

## 6 Summary and discussion

So far, we have demonstrated that a WHWP-SST warming in mid-summer to early fall is able to induce a SST warming and a sea level rise in the WNP in the subsequent winter, not only on an interannual time scale but also on a decadal time scale. This is possible due to active air-sea coupling processes over the subtropical North Pacific which efficiently transmits WHWP signals toward the WNP. CMIP5 models also reasonably simulate such observational dynamical processes. These results imply that WHWP variability have a considerable impact on ecosystem in the WNP.

Since there are numerous studies discussing the equatorial Pacific influence, especially the El Niño Southern Oscillation (ENSO), on the Atlantic (Enfield and Mayer 1997; Alexander and Scott 2002; Chang et al. 2006), one can argue that the above results are diluted by previous or developing El Niño events. However, the relationship between previous/developing El Niño events (Niño3.4 index) and the WHWP index are weak. The correlation coefficients between them are less than 0.2. In the same vein, Zhang and Wang (2012) showed that an El Niño in the preceding winter does not necessarily lead to a large WHWP in the next summer although ENSO variability is, to some extent, associated with a warm pool expansion. In addition, the WHWP index has simultaneously near zero correlation with the Atlantic Niño index, and it is correlated with the NTA index at a marginally significant level (For Atlantic Nino and NTA indices, refer to Ham et al. 2013b). This is because the area of WHWP is partly connected to the NTA as the WHWP expands. However, due to the high climatological WHWP-SST (Wang and Enfield 2003), the WHWP plays a crucial role in the

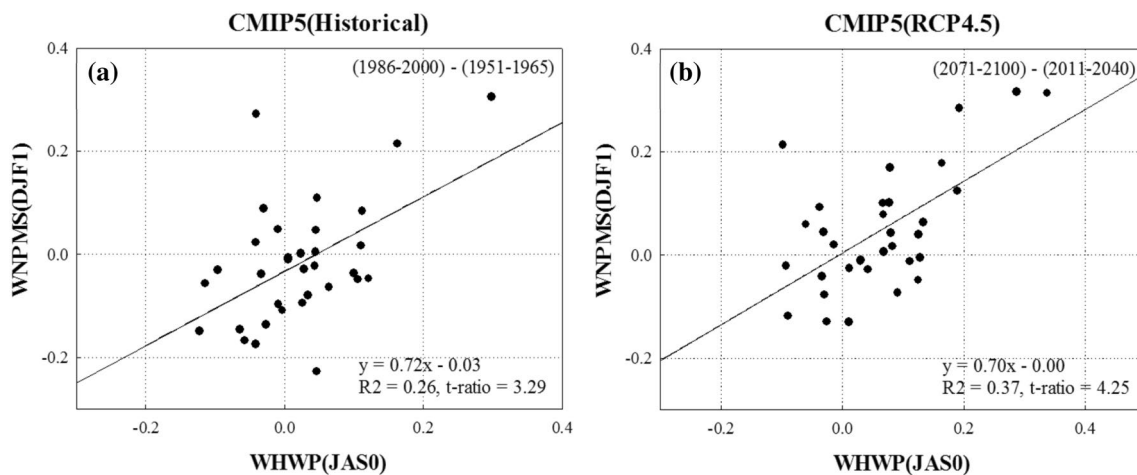


**Fig. 11** **a** A scatter plot of the mean SST difference between two periods (1986–2000 and 1951–1965) in the historical experiment, where each dot corresponds to the result of each model. The X- and Y-axes correspond to summer WHWP-SST (JAS) and winter WNP-

SST (DJF), respectively. **b** Same as panel **a** but with different periods (2071–2100 and 2011–2040) in the RCP4.5 experiment. Note that the global mean SST was removed in the result

modulation of atmosphere. Therefore, it is believed that the WHWP could be a good independent factor for climate research.

The SST pattern over the North Pacific in winter induced by WHWP influence has a similarity with the Victoria Mode (a.k.a. North Pacific Gyre Oscillation), to some extent (Fig. 3g) (Bond et al. 2003; Di Lorenzo et al. 2008). It is known that the atmospheric teleconnection associated with the air-sea coupling in the WNP can form North Pacific oscillation (NPO)/NPGO (Park and An 2014; Park et al. 2017). Thus, this study suggests that the Atlantic, especially WHWP, is closely associated to the primary North Pacific climate mode.

In the meantime, Wang et al. (2012) showed that SST around the Philippines and the Taiwan in winter can be a good precursor of El Niño with one year lag. At this time, current study demonstrated a role of summer WHWP-SST in the following winter WNP-SST variability, implying that WHWP-SST is related to the El Niño with roughly one and half year lag (Park et al. 2018a, b).

Recent studies suggested that the Atlantic may exert a remote impact on the Pacific or global climate. For example, McGregor et al. (2014) suggested that an increase in Atlantic SST contributes to the Walker circulation enhancement and equatorial Pacific cooling. Li et al. (2016) investigated how the Atlantic has affected the overall climate of the Pacific Ocean over the last 30 years. Zhang et al. (2014) showed that NTA-SST can affect tropical Pacific SST via the regional Hadley circulation. It should be noted that while their studies focus more on the decadal to interdecadal scale, this study emphasizes more on interannual to decadal scale.

Meanwhile, Yu et al. (2016) and Ham et al. (2017) pointed out that Atlantic SST anomalies in summer induce anomalous winds in the western Pacific via equatorial Kelvin wave propagation. The atmospheric influence is fast, so largely effective in summer. In contrast, the current study explains the Atlantic effect on Pacific with an emphasis on Rossby wave propagation. However, this effect has a time-delay because of air-sea interaction over the subtropical North Pacific.

Based on the understanding the WHWP-WNP relationship, it is expected that the summer WHWP-SST will be a good indicator of interannual to decadal predictions of WNP climate. Under the observational knowledge that 80% of large (small) warm pools occur during the warm (cool) phases of the AMO (Wang et al. 2008), if AMO experiences its phase shift from positive to negative in the future, there will be a possibility of a mitigated warming trend of SST and a reduced increasing trend of SSH over the WNP.

**Acknowledgements** J.-S. Kug is supported by the Korea Meteorological Administration Research and Development Program under Grant KMI2018-03214, and the National Research Foundation of

Korea(NRF) Grant funded by the Korea government(MSIT) (NRF-2018R1A5A1024958). This work was jointly supported by NSFC grant 41630423, NSF grant AGS-1565653, NOAA NA18OAR4310298, and JAMSTEC JIJI project. This is SOEST contribution number 10641, and IPRC contribution number 1360.

## References

- Alexander M, Scott J (2002) The influence of ENSO on air-sea interaction in the Atlantic. *Geophys Res Lett* 29(14). <https://doi.org/10.1029/2001GL014347>
- An SI, Kim JW, Im SH, Kim BM, Park JH (2012) Recent and future sea surface temperature trends in tropical Pacific warm pool and cold tongue regions. *Clim Dyn* 39:1373–1383
- Behringer DW, Xue Y (2004) Evaluation of the global ocean data assimilation system at NCEP: The Pacific Ocean. In: Eighth symposium on integrated observing and assimilation systems for atmosphere, oceans, and land surface, AMS 84th annual meeting, Washington State Convention and Trade Center, Seattle, Washington, pp 11–15
- Bond NA, Overland JE, Spillane M, Stabeno P (2003) Recent shifts in the state of the North Pacific. *Geophys Res Lett* 30(23):2183. <https://doi.org/10.1029/2003GL018597>
- Carton JA, Giese BS, Grodsky SA (2005) Sea level rise and the warming of the oceans in the Simple Ocean Data Assimilation (SODA) ocean reanalysis. *J Geophys Res* 110:C09006. <https://doi.org/10.1029/2004JC002817>
- Chang P, Fang Y, Saravanan R, Ji L, Seidel H (2006) The cause of the fragile relationship between the Pacific El Niño and the Atlantic Niño. *Nature* 443:324–328
- Chen W, Graf HF, Huang RH (2000) The interannual variability of East Asian Winter Monsoon and its relation to the summer monsoon. *Adv Atmos Sci* 17(1):48–60
- Cheng X, Qi Y, Zhou W (2008) Trends of sea level variations in the Indo-Pacific warm pool. *Glob Planet Chang* 63:57–66
- Chung PH, Li T (2013) Interdecadal relationship between the mean state and El Niño types. *J Clim* 26:361–379
- de Boyer Montégut C, Madec G, Fischer AS, Lazar A, Iudicone D (2004) Mixed layer depth over the global ocean: an examination of profile data and a profile-based climatology. *J Geophys Res Oceans* 109:C12003. <https://doi.org/10.1029/2004JC002378>
- Deser C, Phillips AS, Alexander MA (2010) Twentieth century tropical sea surface temperature trends revisited. *Geophys Res Lett* 37:L10701. <https://doi.org/10.1029/2010GL043321>
- Di Lorenzo E et al (2008) North Pacific Gyre oscillation links ocean climate and ecosystem change. *Geophys Res Lett* 35:L08607. <https://doi.org/10.1029/2007GL032838>
- Enfield DB, Mayer DA (1997) Tropical Atlantic sea surface temperature variability and its relation to El Niño-Southern Oscillation. *J Geophys Res: Oceans* 102:929–945
- Ham YG, Kug JS, Park JY, Jin FF (2013a) Sea surface temperature in the north tropical Atlantic as a trigger for El Niño/Southern oscillation events. *Nat Geosci* 6:112–116
- Ham YG, Kug JS, Park JY (2013b) Two distinct roles of Atlantic SSTs in ENSO variability: North tropical Atlantic SST and Atlantic Niño. *Geophys Res Lett* 40:4012–4017. <https://doi.org/10.1002/grl.50729>
- Ham YG, Chikamoto Y, Kug JS, Kimoto M, Mochizuki T (2017) Tropical Atlantic-Korea teleconnection pattern during boreal summer season. *Clim Dyn* 49:2649–2664
- Hamlington B, Leben R, Strassburg M, Kim KY (2014) Cyclostationary empirical orthogonal function sea-level reconstruction. *Geosci Data J* 1:13–19

- Hartmann DL (2015) Pacific sea surface temperature and the winter of 2014. *Geophys Res Lett* 42:1894–1902
- Huffman GJ, Adler RF, Bolvin DT, Gu G (2009) Improving the global precipitation record: GPCP version 2.1. *Geophys Res Lett* 36:L17808. <https://doi.org/10.1029/2009GL040000>
- Kim S, Kug J-S (2018) What controls ENSO teleconnection to East Asia? Role of western North Pacific precipitation in ENSO teleconnection to East Asia. *J Geophys Res Atmos* 123:10406–10422. <https://doi.org/10.1029/2018JD028935>
- Kistler R, Collins W, Saha S, White G, Woollen J, Kalnay E, Chelliah M, Ebisuzaki W, Kanamitsu M, Kousky V (2001) The NCEP–NCAR 50-year reanalysis: Monthly means CD-ROM and documentation. *Bull Am Meteorol soc* 82:247–267
- Leatherman SP, Zhang K, Douglas BC (2000) Sea level rise shown to drive coastal erosion. *Eos Trans Am Geophys Union* 81:55–57
- Li T, Wang B (2005) A review on the western North Pacific monsoon: synoptic-to-interannual variabilities. *Terr Atmos Oceanic Sci* 16:285–314
- Li X, Xie SP, Gille ST, Yoo C (2016) Atlantic-induced pan-tropical climate change over the past three decades. *Nat Clim Chang* 6:275–279
- Lima FP, WetHEY DS (2012) Three decades of high-resolution coastal sea surface temperatures reveal more than warming. *Nat commun* 3:704
- Liu Z, Gan J (2012) Variability of the Kuroshio in the East China Sea derived from satellite altimetry data. *deep sea research Part I: Oceanographic Res Pap* 59:25–36
- Lysne JA, Deser C (2002) Wind-driven thermocline variability in the Pacific: a model–data comparison. *J Clim* 15:829–845
- McGregor S, Timmermann A, Stuecker MF, England MH, Merrifield M, Jin FF, Chikamoto Y (2014) Recent Walker circulation strengthening and Pacific cooling amplified by Atlantic warming. *Nat Clim Chang* 4:888–892
- Merrifield MA (2011) A shift in western tropical Pacific sea level trends during the 1990s. *J Clim* 24:4126–4138
- Nitta T (1987) Convective activities in the tropical western Pacific and their impact on the Northern Hemisphere summer circulation. *J Meteorol Soc Jap Ser II* 65:373–390
- Park JH, An SI (2014) The impact of tropical western Pacific convection on the North Pacific atmospheric circulation during the boreal winter. *Clim Dyn* 43:2227–2238
- Park JH, An SI, Kug JS (2017) Interannual variability of western North Pacific SST anomalies and its impact on North Pacific and North America. *Clim Dyn* 49:3787–3798. <https://doi.org/10.1007/s00382-017-3538-8>
- Park JH, Kug JS, Li T, Behera SK (2018a) Predicting El Niño–Southern oscillation beyond 1-year Lead: effect of western hemisphere warm Pool. *Sci Rep* 8:14957
- Park JH, Li T, Yeh SW, Kim H (2018b) Effect of recent Atlantic warming in strengthening Atlantic–Pacific teleconnection on interannual timescale via enhanced connection with the Pacific meridional mode. *Clim Dyn* (under revision)
- Qiu B (2003) Kuroshio extension variability and forcing of the Pacific decadal oscillations: responses and potential feedback. *J Phys Oceanogr* 33:2465–2482
- Reynolds RW, Rayner NA, Smith TM, Stokes DC, Wang W (2002) An improved in situ and satellite SST analysis for climate. *J Clim* 15:1609–1625
- Reynolds RW, Smith TM, Liu C, Chelton DB, Casey KS, Schlax MG (2007) Daily high-resolution-blended analyses for sea surface temperature. *J Clim* 20:5473–5496
- Son H-Y, Park J-Y, Kug J-S, Yoo J, Kim C-H (2014) Winter precipitation variability over Korean Peninsula associated with ENSO. *Clim Dyn* 42(11–12):3171–3186
- Vimont DJ, Battisti DS, Hirst AC (2001) Footprinting: a seasonal connection between the tropics and mid-latitudes. *Geophys Res lett* 28:3923–3926
- Vimont DJ, Wallace JM, Battisti DS (2003) The seasonal footprinting mechanism in the Pacific: implications for ENSO. *J Clim* 16:2668–2675
- Wang C, Enfield DB (2001) The tropical Western hemisphere warm pool. *Geophys Res Lett* 28:1635–1638
- Wang C, Enfield DB (2003) A further study of the tropical Western Hemisphere warm pool. *J Clim* 16:1476–1493
- Wang B, Wu R, Fu X (2000) Pacific–East Asian teleconnection: how does ENSO affect East Asian climate? *J Clim* 13:1517–1536
- Wang C, Enfield DB, Lee SK, Landsea CW (2006) Influences of the Atlantic warm pool on Western Hemisphere summer rainfall and Atlantic hurricanes. *J Clim* 19:3011–3028
- Wang C, Lee SK, Enfield DB (2008) Atlantic warm pool acting as a link between Atlantic multidecadal oscillation and Atlantic tropical cyclone activity. *Geochem Geophys Geosyst* 9:Q05V03. <https://doi.org/10.1029/2007GC001809>
- Wang SY, L'Heureux M, Chia HH (2012) ENSO prediction one year in advance using western North Pacific sea surface temperature. *Geophys Res Lett* 39:L05702. <https://doi.org/10.1029/2012GL050909>
- Wang SY, L'Heureux M, Yoon JH (2013) Are greenhouse gases changing ENSO precursors in the Western North Pacific? *J Clim* 26:6309–6322
- Watanabe M, Kimoto M (1999) Tropical-extratropical connection in the Atlantic atmosphere-ocean variability. *Geophys Res Lett* 26:2247–2250
- Whitmarsh F, Zika D, Czaja A (2015) Ocean heat uptake and the global surface temperature record. *Grantham Institute Briefing Paper* 14
- Williams RG (2012) Oceanography: centennial warming of ocean jets. *Nat Clim Chang* 2:149–150
- Wu L, Cai W, Zhang L, Nakamura H, Timmermann A, Joyce T, McPhaden MJ, Alexander M, Qiu B, Visbeck M (2012) Enhanced warming over the global subtropical western boundary currents. *Nat Clim Chang* 2:161–166
- Yeh SW, Kim CH (2010) Recent warming in the Yellow/East China Sea during winter and the associated atmospheric circulation. *Cont Shelf Res* 30:1428–1434
- Yu JY, Kao Pk, Paek H, Hsu HH, Hung CW, Lu MM, An SI (2015) Linking emergence of the central Pacific El Niño to the Atlantic multidecadal oscillation. *J Clim* 28:651–662
- Yu J, Li T, Tan Z, Zhu Z (2016) Effects of tropical North Atlantic SST on tropical cyclone genesis in the western North Pacific. *Clim Dyn* 46:865–877
- Zhang L, Wang C (2012) Remote influences on freshwater flux variability in the Atlantic warm pool region. *Geophys Res Lett* 39(19):19714. <https://doi.org/10.1029/2012GL053530>
- Zhang L, Wang C, Song Z, Lee SK (2014) Remote effect of the model cold bias in the tropical North Atlantic on the warm bias in the tropical southeastern Pacific. *J Adv Model Earth Sys* 6:1016–1026

**Publisher's Note** Springer Nature remains neutral with regard to jurisdictional claims in published maps and institutional affiliations.